

---

P. SARKANYCH,<sup>1</sup> YU. HOLOVATCH,<sup>2</sup> R. KENNA<sup>3</sup>
<sup>1</sup>Department for Theoretical Physics, Ivan Franko National University of Lviv  
(12 Drahomanov St., 79005 Lviv, Ukraine; e-mail: petrosark@gmail.com)

<sup>2</sup>Institute for Condensed Matter Physics of the National Academy of Sciences of Ukraine  
(79011 Lviv, Ukraine)

<sup>3</sup>Applied Mathematics Research Centre, Coventry University  
(Coventry CV1 5FB, UK)

## ON THE PHASE DIAGRAM OF THE 2D ISING MODEL WITH FRUSTRATING DIPOLE INTERACTION

PACS 64.60.De, 75.40.Cx

*Due to intrinsic frustrations of interaction, the 2d Ising model with competing ferromagnetic short-range nearest-neighbour and antiferromagnetic long-range dipole interactions possesses a rich phase diagram. The order of the phase transition from the striped  $h = 1$  phase to the tetragonal phase that is observed in this model has been a subject of recent controversy. We address this question using the partition function density analysis in the complex temperature plane. Our results support the second-order phase transition scenario. To measure the strength of the phase transition we calculate the values of the specific heat critical exponent  $\alpha$ . Along with the space dimension  $D$ , it appears to depend on the ratio of strength of the short-range and long-range interactions.*

*Keywords:* frustrations, phase transition, density of partition function zeros, critical exponents

### 1. Introduction

Pattern formation is one of the fascinating phenomena that may be induced by competing long- and short-range interactions in many-particle physical systems. To give few examples, a competition of short-range and long-range dipole interaction leads to a variety of experimentally observed structures in ultrathin magnetic films on metal substrates, liquid crystals, polymer films, two-dimensional electron gases, Langmuir and lipid monolayers, etc. (see [1] for more detailed references). Being a subject of intensive experimental studies revealing unusual physical effects, the above systems have important industrial applications. In particular, the aforementioned ultrathin magnetic films became a subject of especial interest due to their possible application in creating high-density storage devices [2].

Theoretical insight into peculiarities of pattern formation in the above systems has been gained by analysing the 2d Ising model with competing ferromagnetic short-range nearest-neighbour interactions (with strength given by  $J$ ) and antiferromagnetic long-range dipole interactions (of strength  $g$ ) [1, 3–12]. In the framework of this model, the richness of the phase diagram is attributed to frustrations introduced by the competing character of ferromagnetic and antiferromagnetic interactions. Analytical approaches, supported by numerical simulations, show that, depending on the values of  $J$  and  $g$ , the low temperature phase of this model is characterized by spin configurations classified as regular and irregular checkerboards or stripes of different width  $h$ <sup>1</sup> with spin oriented in similar direction [3–7]. Evidence of modulated phases has been reported for for  $J/g$  ratio

---

<sup>1</sup> Here and below  $h$  is the stripe width measured in lattice units.

near the boundary between striped phases of width  $h$  and  $h + 1$  [11]. The above low-temperature magnetic patterns have much in common with those observed in liquid crystals and the stripped, modulated, and paramagnetic phases are often referred to as smectic, nematic and tetragonal ones. In the latter case, the stripe domains are mutually perpendicular. Moreover, already the mean field analysis reveals that the domain-wall structure in such films is similar to 2d liquid crystals [8].

The papers cited above agree in general on the classification of patterns observed in the 2d Ising model with competing nearest-neighbour and dipole interactions, however the detailed form of the phase diagram remains still unclear. In particular, a subject of recent discussion has been the form of the phase diagram in the region of low values of temperature  $T$  and  $\delta = J/g$  (a sketch of the phase diagram in this region is shown in Fig. 1). Whereas the temperature-induced phase transitions from the antiferromagnetic checkerboard-like phase (AF) and from the striped  $h = 2$  phase to the tetragonal phase are of the second and of the first order, correspondingly, the order of the phase transition between the striped  $h = 1$  phase and the tetragonal phase is the subject of discussion. In particular, MC simulations of Ref. [11] manifest a second order phase transition in the region  $\delta < 0.8$  and the first order transition in the region  $0.83 < \delta < 0.88$ . As a consequence, a tricritical point has been predicted in between the two regions. Subsequent MC simulations of Ref. [12] did not observe the conjectured tricritical point and resulted in the continuous phase transition for all region of  $\delta$  that corresponds to the boundary between the striped  $h = 1$  and tetragonal phases (see Fig. 1). The simulations were supported by the analysis of the partition function zeros in the complex temperature plane (Fisher zeros) [13].

In our study, we will complement analysis of the phase diagram of the 2d Ising model with competing nearest-neighbour and dipole interactions by considering partition function zeros density [14]. In particular, this will allow to avoid a hyperscaling assumption while calculating the strength of the phase transition and directly obtaining the specific heat critical exponent  $\alpha$ . The input data for our analysis are provided by the coordinates of the partition function zeros calculated in [12]. The rest of the paper is organized as follows: in sections 2 and 3 we describe the model

and the method used for its analysis, our results are presented and discussed in section 4.

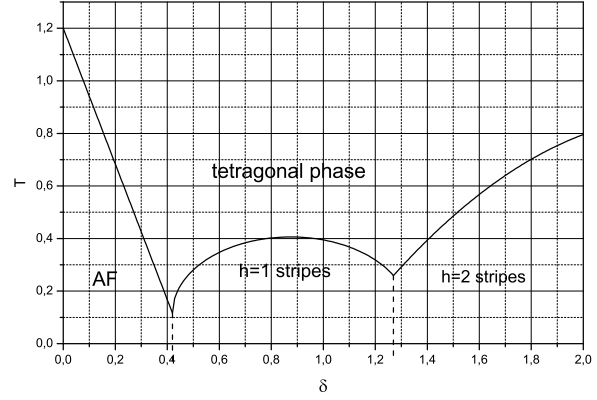


**Fig. 1.** The phase diagram of the 2d Ising model with competing nearest neighbour and dipole interactions (sketched from the Refs. [11, 12]). AF: checkerboard antiferromagnet phase,  $h = 1$ ,  $h = 2$ : striped phases.

## 2. Ising model with dipole interaction

The Hamiltonian of the 2d Ising model with competing ferromagnetic nearest-neighbour and antiferromagnetic dipole interactions reads

$$H = -\delta \sum_{\langle i,j \rangle} \sigma_i \sigma_j + \sum_{i < j} \frac{\sigma_i \sigma_j}{r_{ij}^3}. \quad (1)$$

Here,  $\delta = J/g > 0$ ,  $J$  and  $g$  being strengths of the nearest neighbour and dipole interactions, correspondingly. The summation is performed over the sites of the  $L \times L$  square lattice. The first sum in (1) spans all pairs of nearest-neighbour Ising spins  $\sigma_i = \pm 1$ , while in the second term all pairs of lattice sites are taken into account. The Ising spins are supposed to be aligned out of the plane.

In the limiting cases of  $J = 0$  or  $g = 0$  (i.e.  $\delta$  equals 0 or  $\infty$ ) the Hamiltonian (1) presents a pure dipole interaction model or the usual Ising model, correspondingly. Both cases are characterized by a single (antiferro- or ferromagnetic) low temperature phase and by a continuous second-order phase transition to the paramagnetic state. Note, that the aforementioned antiferromagnetic-to-paramagnetic phase transition belongs to the universality class of the 2d Ising model too [10, 15]. The phase behaviour of the

model (1) is much more complicated for nonzero  $\delta$ , as was briefly described in the introduction. The part of the phase diagram of the model in the region of small  $\delta$  of  $T - \delta$  plane is sketched in Fig. 1.

Previous analyses of the phase diagram were performed either by numerical or analytical tools, based on calculation of the partition function

$$Z_L(\beta) = \text{Tr} \exp(-\beta H), \quad (2)$$

where  $\beta = 1/T$  and the trace is performed over all spin configurations. The analysis we report upon in this paper relies on an examination of the partition function behaviour in the complex  $T$  (complex  $\beta$ ) plane. Since the pioneering papers of Lee and Yang [16] and Fisher [13] where the partition function zeros in complex field and complex temperature planes were studied, this type of analysis became a powerful tool to study phase transitions in various models. For the model under consideration (1) it has been recently applied in Ref. [12], where the first zero of the partition function closest to the origin has been calculated for different values of interaction ratio  $\delta$  at different lattice sizes  $L = 12 - 72$ . The finite size scaling (FSS) analysis of the zeros' coordinates allows one to obtain the value of the correlation length critical exponent  $\nu$ . The value of  $d\nu$  is given in Table 1 for different values of  $\delta$ . Provided that the hyperscaling relation  $\alpha = 2 - d\nu$  holds, one can use it to obtain the specific heat critical exponent  $\alpha$ . Corresponding  $\alpha(\delta)$  values are quoted in the third column of the Table 1. Since  $\alpha = 1$  for first-order phase transitions, the obtained values of the exponents  $\alpha < 1$  serve an evidence for a second-order phase transition in the considered region of  $\delta$ . This result has been further supported by a FSS analysis of the specific heat, leading to the ratio  $\alpha/\nu$  that is quoted in the fourth column of Table 1 [12]. Again, using the hyperscaling relation one can extract the value of the  $\alpha$  at  $d = 2$  via:  $\alpha = \frac{2\alpha/\nu}{d+\alpha/\nu}$ . The last value is shown as a function of  $\delta$  in the fifth column of the table.

We note that, although the above-obtained estimates for  $\alpha$  support a continuous phase-transition scenario ( $\alpha < 1$ ), they do not agree numerically. Moreover, the methods used for their determination do not deliver their direct evaluation, but rather rely on hyperscaling relations. Therefore, in the forthcoming section we will use an alternative partition-

function-zeros analysis that allows direct determination of the exponent  $\alpha$ .

### 3. Density of partition function zeros

In our analysis we will use the method of analysing the density of partition function zeros originally suggested in [14]. A particular advantage of this method is that it allows to discriminate between the first- and second-order (as well as higher order) phase transitions as well as to measure the strength of first- and second-order phase transitions in the form of the latent heat and critical exponents. Below we briefly describe the main steps of the partition function density analysis. Provided that the zeros of the partition function of the model (given by (2) in our particular case) in the complex plane are known, one can write it in the factorized form

$$Z_L(z) = A(z) \prod_j (z - z_j(L)) \quad , \quad (3)$$

where  $z$  stands generically for an appropriate function of complex temperature (in the Fisher case) or complex field (in the Lee-Yang case),  $L$  is the linear extent of the lattice and  $A(z)$  is a smooth function that never vanishes. The free energy density follows as

$$\begin{aligned} f_L(z) &= \frac{1}{L^d} \ln Z_L(z) \\ &= \frac{1}{L^d} \left( \ln A(z) + \sum_j \ln(z - z_j(L)) \right). \end{aligned} \quad (4)$$

The first term on the right contributes only to the regular part of thermodynamic functions and will be dropped henceforth. The remainder, which will be referred to as  $f_L^s(z)$ , gives rise to singular behaviour.

It is suitable to parameterize the zeros by

$$z = z_c + r \exp(i\varphi), \quad (5)$$

where  $z_c$  is a critical point coordinate. Let us define the density of zeros as

$$g_L(r) = L^{-d} \sum_j \delta(r - r_j(L)), \quad (6)$$

with  $z_j = z_c + r_j \exp(i\varphi)$ . Subsequently, the free energy and the cumulative distribution function of zeros are defined as

$$f_L^s(z) = \int_0^R g_L(r) \ln(z - z_c - r e^{i\varphi}) dr + \text{c.c.} \quad , \quad (7)$$

$\delta$	$d\nu$ [12]	$\alpha = 2 - d\nu$	$\alpha/\nu$ [12]	$\alpha = \frac{2\alpha/\nu}{d+\alpha/\nu}$	$\alpha_{zd}$
0.89	1.807(70)	0.193(70)	0.364(20)	0.308(17)	0.194(17)
0.91	1.817(68)	0.183(68)	0.375(19)	0.316(16)	0.191(14)
0.93	1.779(61)	0.221(61)	0.399(20)	0.333(17)	0.221(16)
0.95	1.741(53)	0.259(53)	0.424(20)	0.350(17)	0.255(14)
0.97	1.706(46)	0.294(46)	0.461(19)	0.375(16)	0.292(14)
1.00	1.659(37)	0.341(37)	0.522(17)	0.414(14)	0.349(13)
1.10	1.415(25)	0.585(25)	0.888(21)	0.615(15)	0.5882(84)
1.20	1.223(21)	0.777(21)	1.496(28)	0.856(16)	0.788(17)
1.30	1.0093(28)	0.9907(28)	2.0183(66)	1.0046(33)	1.011(13)

Table 1. Critical exponents of the 2d Ising model with competing ferromagnetic nearest-neighbour and antiferromagnetic dipole interactions for different values of the interaction ratio  $\delta$ . Results of Ref. [12] obtained by FSS of the partition function zeros and of the specific heat,  $d\nu$  and  $\alpha/\nu$  are shown in the second and fourth columns, respectively. The specific heat critical exponents  $\alpha$  obtained via hyperscaling relations from these values are given in the third and in the fifth columns, correspondingly. The sixth column contains our results obtained via the partition function zeros density analysis ( $\alpha_{zd}$ ).

$$G_L(r) = \int_0^r g_L(s)ds = \begin{cases} = \frac{j}{L^d} & \text{if } r \in (r_j, r_{j+1}) \\ = \frac{2j-1}{2L^d} & \text{if } r = r_j \end{cases} \quad (8)$$

where c.c. means complex conjugate and  $R$  is some appropriate cutoff. In the thermodynamic limit and for first order phase transitions, Lee and Yang already have shown [16] that the density of zeros has to be non-zero crossing the real axis. This corresponds to the cumulative distribution of zeros

$$G_\infty(r) = g_\infty(0)r + br^{w+1} + \dots, \quad (9)$$

where the slope at the origin is related to the latent heat (or magnetization) via

$$\Delta e \propto g_\infty(0). \quad (10)$$

Furthermore, it has been shown (see [17, 18]) that the necessary and sufficient condition for the specific heat at second-order phase transitions to have the leading critical behaviour  $C \sim t^{-\alpha}$ , is

$$G_\infty(r) \propto r^{2-\alpha}. \quad (11)$$

The above survey leads to the conclusions that a plot of  $G_L(r_j) = (2j-1)/2L^d$  against  $r_j(L)$  should: (i) go through the origin, (ii) display  $L$ - and  $j$ -collapse, and (iii) reveal the order and strength of the

phase transition by its slope near the origin. In the next section we will give results of an analysis of corresponding plots for the partition function (2) of the model with the Hamiltonian (1).

#### 4. Results and conclusions

As it has been stated in the Introduction, the input data for our analysis are provided by the coordinates of the partition function zeros calculated in [12] for different  $\delta$  and  $L$ . From these, we calculate  $G(r)$  dependence of the cumulative density function (8) for different values of  $\delta$ . Obtained in this way, a typical  $G(r)$  plot is shown in Fig. 2 for  $\delta = 1$ . Subsequently, the set of functions  $G(r)$ , for every value of  $\delta$ , is fitted with  $G(r) = ar^{2-\alpha} + b$ . The resulting values of the specific heat critical exponent are listed in the last column of Table 1,  $\alpha_{zd}$ .

There are several conclusions one can make comparing the data for the specific heat exponents from Table 1. First of all it is worth noting that the results obtained by three different techniques: (i) FSS of partition function zeros (third column of the table, obtained by hyperscaling relation from data of Ref. [12]), (ii) FSS of the specific heat [12] (fifth column of the table) and (iii) density of partition function zeros analysis (last column of the table, our data) give value of  $\alpha < 1$  up to  $\delta < 1.3$ . Recalling that that  $\alpha = 1$  serves as evidence for a first-order phase transition (cf. Eqs. (7) and (9)) one can conclude that the transition from the striped  $h = 1$  to the tetragonal phase

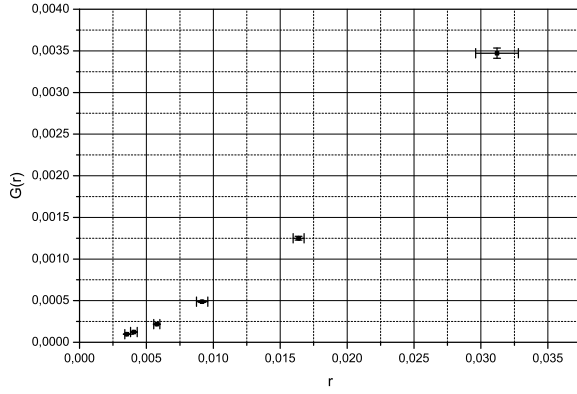


**Fig. 2.** Cumulative density function  $G(r)$  for  $\delta = 1$ .

(see the phase diagram Fig. 1) occurs through a continuous transition scenario. For the values of  $\delta \geq 1.3$  all three approaches predict a first-order phase transition, leading to the conclusion that the tricritical point is located in region  $1.2 < \delta < 1.3$ .

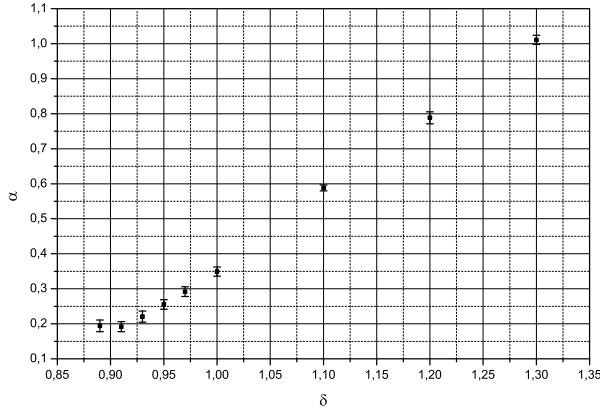


**Fig. 3.** Dependency of the critical exponent  $\alpha$  calculated in this study ( $\alpha_{zd}$ ) on the interaction parameter  $\delta$ .

All three approaches deliver  $\delta$ -dependent values of the critical exponents, making  $\delta$  along with the space dimension  $d$  the global variable that defines the universality class. Dependency of the critical exponent  $\alpha$  calculated in this study ( $\alpha_{zd}$ ) on the interaction parameter  $\delta$  is shown in Fig. 3. Let us note however, that the numerical values of the exponents obtained via different approaches differ. In particular,

results of the FSS analysis of partition function zeros (third column of the table) are in good agreement with the analysis of the density of partition function zeros (sixth column of the table). But they essentially differ from the results obtained on the basis of a FSS analysis of the specific heat behaviour [12]. This result calls for further investigation.

This work is supported in part by FP7 Marie Curie Action grants PIRSES-GA-2011- 295302-SPIDER and PIRSES-GA-2010-269139 - DCP-PhysBio. P.S. acknowledges useful discussion during the young scientists conference at the Bogolyubov Institute for Theoretical Physics (Kyiv, Ukraine, December 24-27, 2013) where this work was presented.

1. A. Giuliani, J.L. Lebowitz, E.H. Lieb, Phys. Rev. B **74**, 064420 (2006).
2. D. Pescia and V.L. Pokrovsky, Phys. Rev. Lett. **65**, 2599 (1990).
3. A. B. MacIsaac, J. P. Whitehead, M. C. Robinson, and K. De'Bell, Phys. Rev. B **51**, 16033 (1995).
4. Ar. Abanov, V. Kalatsky, V. L. Pokrovsky, and W. M. Saslow, Phys. Rev. B **51**, 1023 (1995).
5. I. Booth, A. B. MacIsaac, J. P. Whitehead, and K. De'Bell, Phys. Rev. Lett. **75**, 950 (1995).
6. Vaterlaus et al., Phys. Rev. Lett. **84**, 2247 (2000).
7. S. A. Cannas, D. A. Stariolo, and F. A. Tamarit, Phys. Rev. B **69**, 092409 (2004).
8. A. B. Kashuba and V. L. Pokrovsky, Phys. Rev. B **48**, 10335 (1993).
9. P. M. Gleiser, F. A. Tamarit, and S. A. Cannas, Physica D 168-169, **73** (2002).
10. E. Rastelli, S. Regina, and A. Tassi, Phys. Rev. B **73**, 144418 (2006).
11. E. Rastelli, S. Regina, and A. Tassi, Phys. Rev. B **76**, 054438 (2007).
12. J. S. M. Fonseca, L. G. Rizzi, and N. A. Alves, Phys. Rev. E **86**, 011103 (2012).
13. M.E. Fisher, in: Lecture in Theoretical Physics, Vol. VIIC, ed. W.E. Brittin (Gordon and Breach, New York, 1968); p. 1.
14. W. Janke and R. Kenna, J. Stat. Phys. **102**, 1211 (2001).
15. A. B. MacIsaac, J. P. Whitehead, K. De'Bell, and K. S. Narayanan, Phys. Rev. B **46**, 6387 (1992).
16. C.N. Yang and T.D. Lee, Phys. Rev. **87** (1952) 404; ibid. 410.
17. R. Abe, Prog. Theor. Phys. **37** (1967) 1070; Prog. Theor. Phys. **38** (1967) 72; ibid. 322; ibid. 568.
18. M. Suzuki, Prog. Theor. Phys. **38** (1967) 289; ibid. 1225; ibid. 1243; Prog. Theor. Phys. **39** (1968) 349.

19. C. Itzykson, R. B. Pearson, and J. B. Zuber, Nucl. Phys. B **220** [FS8], 415 (1983).

Received